JPn Neuroscience
The Journal of Physiology

Heterogeneous properties of central lateral and parafascicular thalamic synapses in the striatum

T. J. Ellender, J. Harwood, P. Kosillo, M. Capogna and J. P. Bolam

MRC Anatomical Neuropharmacology Unit, Department of Pharmacology, Mansfield Road, Oxford OX1 3TH, UK

Key points

- The excitatory afferents to the striatum from the cortex and thalamus are critical in the expression of basal ganglia function.
- Thalamostriatal afferents are markedly heterogeneous and arise in different subnuclei of the intralaminar thalamus.
- We used an optogenetic approach, to isolate and selectively activate thalamostriatal afferents arising in the central lateral or parafascicular thalamic nuclei, and to study the properties of their synapses with principal striatal neurons, the medium-spiny neurons.
- Thalamostriatal synapses differ in many aspects and our data suggest that inputs from the central lateral nucleus are efficient drivers of medium-spiny neuron action potential firing, whereas inputs from the parafascicular nucleus are likely to be modulatory.
- These results suggest distinct roles for thalamostriatal inputs from different subnuclei of the thalamus and will help us understand how the striatal circuit operates in health and disease.

Abstract To understand the principles of operation of the striatum it is critical to elucidate the properties of the main excitatory inputs from cortex and thalamus, as well as their ability to activate the main neurons of the striatum, the medium spiny neurons (MSNs). As the thalamostriatal projection is heterogeneous, we set out to isolate and study the thalamic afferent inputs to MSNs using small localized injections of adeno-associated virus carrying fusion genes for channelrhodopsin-2 and YFP, in either the rostral or caudal regions of the intralaminar thalamic nuclei (i.e. the central lateral or parafascicular nucleus). This enabled optical activation of specific thalamic afferents combined with whole-cell, patch-clamp recordings of MSNs and electrical stimulation of cortical afferents, in adult mice. We found that thalamostriatal synapses differ significantly in their peak amplitude responses, short-term dynamics and expression of ionotropic glutamate receptor subtypes. Our results suggest that central lateral synapses are most efficient in driving MSNs to depolarization, particularly those of the direct pathway, as they exhibit large amplitude responses, short-term facilitation and predominantly express post-synaptic AMPA receptors. In contrast, parafascicular synapses exhibit small amplitude responses, short-term depression and predominantly express postsynaptic NMDA receptors, suggesting a modulatory role, e.g. facilitating Ca^{2+}-dependent processes. Indeed, pairing parafascicular, but not central lateral, presynaptic stimulation with action potentials in MSNs, leads to NMDA receptor- and Ca^{2+}-dependent long-term depression at these synapses. We conclude that the

J. Harwood and P. Kosillo contributed equally.

DOI: 10.1113/jphysiol.2012.245233

main excitatory thalamostriatal afferents differ in many of their characteristics and suggest that they each contribute differentially to striatal information processing.

(Resubmitted 20 September 2012; accepted after revision 21 October 2012; first published online 29 October 2012)
Corresponding author T. J. Ellender: MRC Anatomical Neuropharmacology Unit, Department of Pharmacology, Mansfield Road, Oxford OX1 3TH, UK. Email: tommas.ellender@pharm.ox.ac.uk

Abreviations AAV2, adeno-associated virus serotype 2; A/D, analog/digital; ACSF, artificial cerebrospinal fluid; CA3, CA3 field of the hippocampus; CAMKII, Ca^{2+}/calmodulin-dependent protein kinase II; ChR2, channelrhodopsin-2; ChETA, channelrhodopsin-2 E123T accelerated variant; CL, central lateral; D1, dopamine receptor 1; D2, dopamine receptor 2; D-AP5, D-(−)-2-amino 5-phosphonopentanoic acid; DG, dentate gyrus; DIC, differential interference contrast; EC, external capsule; fr, fasciculus retroflexus; GFP, green fluorescent protein; Lhb, lateral habenula; LED, light-emitting diode; LTS, low threshold spike; LV, lateral ventricle; Mhb, medial habenula; MK-801, (5*S*,10*R*)-(+)-5-methyl-10,11-dihydro-5*H*-dibenzo[a,d]cyclohepten-5,10-imine maleate; MSN, medium-sized spiny neuron; mt, mammillothalamic tract; NDS, normal donkey serum; PBS, phosphate buffered saline; Pf, parafascicular; PPE, preproenkephalin; PPR, paired-pulse ratio, YFP, yellow fluorescent protein.

Introduction

The basal ganglia are a group of subcortical brain nuclei essential for the control of movement and a variety of other functions (Graybiel *et al.* 1994; Grillner *et al.* 2005; Yin & Knowlton, 2006). The striatum is the main input nucleus of the basal ganglia receiving excitatory afferents from the cortex and the thalamus (Kemp & Powell, 1971; Buchwald *et al.* 1973; Smith *et al.* 2004). The main thalamic afferents to the striatum originate in the intralaminar nuclei (Macchi *et al.* 1984), which in rodents, can be divided into the rostral central lateral (CL) and the caudal parafascicular (Pf) nucleus (Berendse & Groenewegen, 1990; Castle *et al.* 2005; Smith *et al.* 2009). Both thalamic projections make direct synaptic contacts with the main classes of medium spiny neuron (Xu *et al.* 1991; Sadikot *et al.* 1992; Lacey *et al.* 2007). The Pf afferents, moreover, make contact with several types of striatal interneuron (Lapper & Bolam, 1992; Rudkin & Sadikot, 1999; Sidibé & Smith, 1999). Behavioural studies, mainly focused on Pf, have suggested thalamic intralaminar involvement in a variety of processes (Van der Werf *et al.* 2002; Smith *et al.* 2004; Minamimoto *et al.* 2005), including conveying behaviourally significant sensory signals (Matsumoto *et al.* 2001) and attentional values (Kinomura *et al.* 1996) to the striatum.

Although the thalamostriatal and corticostriatal pathways give rise to similar numbers of synapses on MSNs (Lacey *et al.* 2005; Fujiyama *et al.* 2006; Raju *et al.* 2006; Moss & Bolam, 2008; Doig *et al.* 2010), the properties of thalamostriatal synapses have proven difficult to study because of the heterogeneity of the projection and the trajectory of the axons connecting the thalamus and striatum. The latter can be overcome, to some extent, when studying the projection as a single entity, by careful placement of stimulating electrodes and/or careful selection of the slicing plane *in vitro* (Ding *et al.* 2008; Smeal *et al.* 2008). However, electrical stimulation cannot isolate different subnuclei of the thalamostriatal system. It is clear that these have different properties; for instance, it has been shown that thalamostriatal neurons in the CL and Pf nuclei differ in their morphology, firing properties, as well as their striatal targets (Lacey *et al.* 2007), presumably underlying different roles in striatal function.

The aim of the work described in this paper was to test the hypothesis that synapses formed in the striatum by neurons originating in different subnuclei of the intralaminar thalamus have different functional properties. To address this we set out to isolate and selectively activate the thalamostriatal projection originating in either the rostral or caudal portion of the intralaminar nuclei using targeted viral delivery of channelrhodopsin-2 (ChR2) (Boyden *et al.* 2005). Whole-cell patch-clamp recordings of neurochemically identified MSNs together with optical activation of these specific thalamic inputs enabled us to identify the properties of the two types of thalamic synapse, as well as electrically activated cortical synapses, in the adult mouse striatum. We conclude that thalamostriatal synapses with striatal principal neurons show a hitherto unidentified heterogeneity which suggests they subserve different roles in striatal computation.

Methods

Animals

All experiments were carried out on transgenic mouse lines which were bred and housed in accordance with the Animals (Scientific Procedures) Act 1986. Recordings were carried out on CAMKII-cre mice which express cre recombinase in all CAMKII expressing neurons and were obtained from Jackson laboratory and kept as a homozygous breeding line.

Viral transfection

Adeno-associated virus serotype 2 (AAV2) carrying fusion genes for ChR2 or ChETA and YFP were injected into thalamus or cortex of CAMKII-cre mice between postnatal day 14 and 21. CAMKII is expressed in excitatory (glutamatergic) neurons and these transgenic mice generate cre recombinase in excitatory neurons, including corticostriatal and thalamostriatal neurons. Either the rostral intralaminar nuclei (mostly CL) or caudal intralaminar nuclei (mostly Pf) were targeted. Typical coordinates from Bregma for rostral intralaminar nuclei injections were lateral, 0.6 mm; posterior, 1.4 mm; and 3.1 mm depth from surface of brain. Typical coordinates from Bregma for caudal intralaminar nuclei injections were lateral, 0.7 mm; posterior, 2.4 mm; and 3.5 mm depth from surface of brain. Typical coordinates from Bregma for cortical injections were lateral, 0.7 mm; posterior, 0.1 mm; and 0.3 mm ventral to the surface of brain. Briefly, CAMKII-cre mice were anaesthetized with isoflurane (2–4% in oxygen) and given analgesics (~20 μl of 1:10 dilution of 0.3 mg ml^{-1} buprenorphine solution; Vetergesic; RHS, Slough, UK). A small craniotomy was made over the injection location. Viral particles were delivered through a 33-gauge needle using a Hamilton Microliter syringe placed in a Micro Syringe Pump Controller (Micro4, WPI) at a rate of 0.1 μl min^{-1}. Injection volumes were 300 nl. Following a 3 min wait after injection the needle was retracted by 0.2 mm and, after another 3 min wait, slowly and fully retracted and the skin sutured. Topical analgesics were applied to the skin around the suture (Marcain) and subcutaneous injection of 5% glucose-saline solution given. Viral DNA included the double-floxed sequence for ChR2(H134R)-EYFP or ChR2(E123T-H134R)-EYFP driven by the elongation factor 1 promoter. AAV2 particles were produced at the University of North Carolina Gene Therapy Center Virus Vector Core. Typical titers were ~10^{12} IU ml^{-1}. After allowing 6–12 weeks for ChR2 or ChETA expression, acute striatal slices were prepared. Initial experiments to determine the correct injection coordinates and injection procedure consisted of injections of red latex beads (Lumafluor) together with immunostaining for cerebellin-1.

Slice preparation

Oblique coronal striatal slices (300–400 μm) were prepared from 2 to 4-month-old injected CAMKII-cre mice. Mice were anaesthetized with isoflurane (2–4% in oxygen) and decapitated. Slices were prepared in artificial cerebrospinal fluid (ACSF) containing (in mM): 130 NaCl, 3.5 KCl, 1.25 NaH_2PO_4, 5 $MgCl_2$, 2.5 $CaCl_2$, 24 $NaHCO_3$, and 10 glucose, pH 7.2–7.4, bubbled with carbogen gas (95% O_2–5% CO_2). Slices were immediately transferred to a storage chamber containing ACSF (in mM): 130 NaCl, 3.5 KCl, 1.25 NaH_2PO_4, 1.5 $MgCl_2$, 2.5 $CaCl_2$, 24 $NaHCO_3$, and 10 glucose, pH 7.2–7.4, bubbled with carbogen gas, at 37°C for 30 min and subsequently maintained at room temperature until used for recording.

Recording

Whole-cell current-clamp and voltage-clamp recordings from dorsal striatal MSNs were performed using glass pipettes, pulled from standard wall borosilicate glass capillaries containing, for whole-cell current-clamp (in mM): 110 potassium gluconate, 40 HEPES, 2 ATP-Mg, 0.3 Na-GTP, 4 NaCl and 4 mg ml^{-1} biocytin (pH 7.2–7.3; osmolarity, 290–300 mosmol l^{-1}); and for whole-cell voltage-clamp (in mM): 120 caesium gluconate, 40 HEPES, 4 NaCl, 2 ATP-Mg, 0.3 Na-GTP, 0.2 QX-314 and 4 mg ml^{-1} biocytin (pH 7.2–7.3; osmolarity, 290–300 mosmol l^{-1}). In a subset of synaptic plasticity experiments either EGTA (10 mM) or MK-801 (1 mM) was included in the current-clamp internal solution. All recordings were made using an EPC9/2 HEKA amplifier with integrated A/D converter and acquired using Pulse software (HEKA Electronik). All recordings were performed at 32°C.

Stimulation and recording protocols

MSN afferents were stimulated electrically and optically. Electrical stimulation was performed by placing an ACSF filled glass electrode in the external capsule for activation of corticostriatal afferents. Stimulation strength was set to evoke approximately 1/3 of maximum response corresponding to a stimulation strength of 100–300 μA and 0.1 ms duration. Optical stimulation of thalamostriatal or corticostriatal afferents was performed using the optoLED system (Cairn Research), consisting of a 470 nm, 3.5 W LED mounted on a Zeiss Axioskop 2 FS microscope, to give 3 ms duration light pulses of ~5% of maximum output power. The steady-state light power at the tissue was measured using a PMD100D power metre and photodiode sensor (Thor Labs). The spot size corresponded to the area of the slice visualized using a 40×/0.8NA water immersion objective, i.e. approximately 220 μm diameter. In some experiments we attempted to stimulate single thalamic afferents with a 473 nm diode laser (max. 100 mW output; UGA-40; Rapp OptoElectronic) coupled to the microscope with a single mode optic fibre (S405; Thorlab; 10 μm diameter spot; 3 ms duration pulses). Activation of excitatory afferents was performed in the presence of blockers of inhibitory GABAergic transmission including the $GABA_A$-receptor antagonist SR95331 (10 μm) and $GABA_B$-receptor antagonist CGP52432 (2 μm). Fibres were activated every 10 s and excitatory postsynaptic

currents (EPSCs) or excitatory postsynaptic potentials (EPSPs) were recorded in the patched MSN. Evoked EPSCs were recorded in whole-cell voltage-clamp mode at a holding potential near −80 mV and evoked EPSPs in whole-cell current-clamp mode at resting membrane potential. For paired-pulse stimulation, two stimulating pulses were consecutively given at 50 ms interval and repeated every 10 s for up to 20 times. Trains of pulses consisted of nine pulses at 5, 10 and 20 Hz, with the latter two followed by a recovery pulse 500 ms later, and was repeated every 30 s for up to 5 times. Combined AMPA and NMDA receptor-mediated currents were recorded from MSNs held at +40 mV. AMPA receptor-mediated currents were recorded after 5 min wash-in of D-AP5 (50 μm). Both consisted of at least 20 evoked responses at 0.1 Hz. The pairing-induced plasticity protocol consisted of pairing presynaptic activation of thalamic afferents with a single postsynaptic action potential in MSNs, induced by a suprathreshold current step (1 nA, 10 ms), with approximately 8 ms time difference. After a 5 min baseline recording of EPSPs at 0.1 Hz the pairing protocol was repeated 100 times at 1 Hz. Subsequently EPSPs were recorded for 25 min at 0.1 Hz.

Analysis of intracellular recordings

Data was analysed offline using custom written procedures in Igor Pro (Wavemetrics). EPSCs or EPSPs were defined as upward or downward deflections of more than 2 standard deviations (SD) above baseline. Paired-pulse ratios were calculated by dividing the average slope of the second EPSC (S2) with the average slope of the first EPSC (S1). In plasticity experiments the paired-pulse ratio was determined prior to the induction protocol and at the end of the recording. Slopes of individual EPSCs were determined between 20% and 80% of maximum EPSC amplitude. Trains were analysed by taking the amplitude of each EPSC and dividing this by the amplitude of the first EPSC. The analysis of EPSC and EPSP basic properties (peak amplitude, duration, rise time (between 20% and 80% from peak) and decay time) was performed on individual synaptic responses. EPSCs obtained using minimal stimulation were defined as downward deflections of more than 3 standard deviations (SD) above baseline. NMDA/AMPA ratios were calculated from an average trace of combined AMPA and NMDA receptor-mediated currents and AMPA receptor-mediated currents. The average AMPA receptor-mediated current trace was subtracted from the combined AMPA and NMDA receptor-mediated current trace to obtain the NMDA receptor-mediated current. The maximum amplitude of the NMDA receptor-mediated current was divided by the maximum amplitude of the AMPA receptor-mediated current to obtain the NMDA/AMPA ratio. In plasticity experiments the average amplitude of every two consecutive EPSPs was plotted. Plastic changes at synapses were assessed by comparing the average amplitude of recorded EPSPs during the last five minutes post induction with the baseline. The input resistance was constantly monitored by applying short –200 pA current steps to the patch pipette. If the input resistance changed more than 20% the recording was discarded.

Histological analyses

Following intracellular recording, the slices were fixed overnight in 4% paraformaldehyde and 15% saturated picric acid in 0.1 M phosphate buffer (PB; pH 7.4) at 4°C. After washes the slices were embedded in 5% agar and resectioned at 50 μm on a vibrating microtome (VT1000S; Leica Microsystems). All sections were pre-incubated in 10%-20% normal donkey serum (NDS; Vector Laboratories) in PBS for more than 1 h at room temperature. Biocytin-filled cells were visualized by incubating sections in 1:10,000 streptavidin-405 conjugate (Invitrogen) in PBS containing 0.3% Triton X-100 (PBS-Tx) overnight at 4°C. YFP expression in thalamic fibres was visualized by incubating sections in 1:1000 chicken anti-GFP (Aves Labs) in PBS-Tx and 1% NDS overnight at 4°C followed by 1:500 donkey-anti-chicken-488 fluophore (Jackson Immunoresearch Laboratories) in PBS-Tx for 2 h at room temperature. To define the subtype of recorded MSN, the sections were heated at 80°C in 10 mM sodium citrate (pH 6.0) for approximately 30 min prior to incubation with 1:1000 rabbit anti-preproenkephalin (LifeSpan biotechnology) in PBS-Tx and 1% NDS overnight at 4°C after which the reaction was revealed by incubating with 1:500 donkey-anti-rabbit-Cy3 fluophore (Jackson Immunoresearch Laboratories) in PBS-Tx for 2 h at room temperature. The neurons that were immunopositive were classified as indirect pathway MSNs.

To confirm the AAV injection was correctly localized in the thalamic intralaminar nuclei, following preparation of the slices for recording, the remainder of the brain, containing thalamus, was immersion fixed overnight in 4% paraformaldehyde and 15% saturated picric acid in 0.1 M phosphate buffer (PB; pH 7.4) at 4°C. After washes, the brain blocks were resectioned at 50 μm on a vibrating microtome (VT1000S; Leica Microsystems). The sections were incubated in 20% NDS (Vector Laboratories) for 45 min at room temperature. A subset of sections was heated at 80°C in 10 mM sodium citrate (pH 6.0) for approximately 30 min prior to incubation with 1:2500 rabbit-anti-cerebellin-1 (Wei *et al.* 2007) In all sections YFP was visualised by immunolabelling using 1:1000 chicken-anti-GFP (Aves

Labs) in PBS-Tx and 1% NDS overnight at 4°C followed by 1:500 donkey-anti-chicken-488 fluophore (Jackson Immunoresearch Laboratories), and in a subset of sections, 1:500 donkey-anti-rabbit-Cy3 fluophore (Jackson Immunoresearch Laboratories), in PBS-Tx for 2 h at room temperature. To facilitate anatomical characterization, the sections were incubated for 30 min in a 1:200 Nissl-Cy5 stain (Neurotrace, Invitrogen). Finally, all sections were mounted in Vectashield (Vector Laboratories) and images were captured with a LSM 710 (Zeiss, Göttingen, Germany) confocal microscope using ZEN and Axiovision software (Zeiss, Göttingen, Germany). The software's default settings for fluorophores were used for beamsplitters and ranges of emissions sampled.

Statistics

All data are presented as means ± SEM, except where stated. Student's *t* test, Wilcoxon's signed-rank test and the Mann–Whitney *U* test were performed using SPSS 17.0 ($^{*}P < 0.05$, $^{**}P < 0.01$).

Drugs and chemicals

All drugs were obtained from Tocris Biosciences (Bristol, UK) and Sigma-Aldrich (Poole, Dorset, UK).

Results

Localized transfection of CL or Pf thalamic neurons

The main thalamic input to the striatum comes from the rostral (central lateral) and caudal (parafascicular) region of the intralaminar nuclei (Macchi *et al.* 1984), which have distinct morphological and electrophysiological properties (Lacey *et al.* 2007). We set out to characterize these different inputs to MSNs by using small volume (300 nl) injections of AAV2 containing the double-floxed sequence for the light activatable channel ChR2 in either the rostral or caudal portion of the intralaminar nuclei of CAMKII-cre mice (Fig. 1*A* and *B*). These transgenic mice generate cre recombinase in all CAMKII-expressing neurons and this approach allows expression of the light activatable channel only in the excitatory thalamic neurons around the site of injection. The AAV used is replication deficient and AAV serotype 2 was chosen, over e.g. AAV serotype 5, as it has been shown to enable focal neuronal transfection (Burger *et al.* 2004). After an initial iterative process, consisting of injections of latex beads in different locations (Supplemental Fig. S1*A*) and assessing the spread of the AAV transfection using different injection volumes in combination with immunolabelling of the thalamic nuclei (Wei *et al.* 2007) (Supplemental Fig. S1*B*),

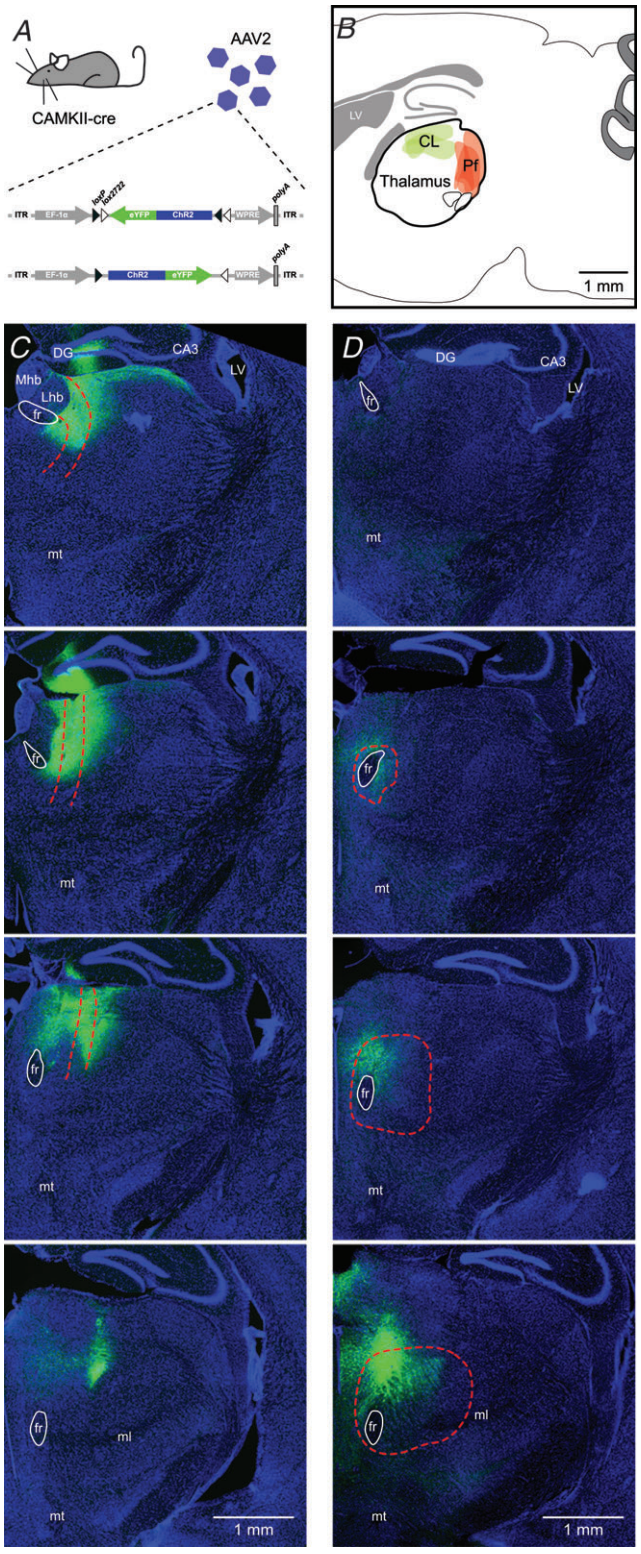

Figure 1. Localized transfection of neurons in the central lateral or parafascicular thalamic nucleus
A, AAV particles containing the double-floxed sequence for the light activatable channel, channelrhodopsin-2 and YFP were injected into the thalamic intralaminar nuclei. Infected neurons expressing cre-recombinase under the CAMKII promoter will start expressing

we were able to selectively inject either nucleus with little overlap, as assessed by the localization of YFP-expressing neurons (Fig. 1*C* and *D*). This suggests that transfection was predominantly localized to the CL or Pf subnuclei of the intralaminar thalamus. The transfected thalamic neurons for both nuclei covered an anterioposterior distance of approximately ~750 μm (CL; 764 ± 85 μm and Pf; 706 ± 66 μm; $n = 7$ and 8), consistent with previous reports (Cardin *et al.* 2009). Although we found little to no transfection of cortical neurons we did find, particularly for rostral injections, occasional transfection of hippocampal neurons, but as the hippocampal projection is predominantly to ventral striatum we did not see this as a major issue.

MSNs receive both thalamic and cortical input

Following a survival time of 6–12 weeks, brain slices of the forebrain were prepared from injected CAMKII-cre mice. The relatively long survival time enables sufficient expression of ChR2 throughout the axonal arbor of the thalamic neurons, including their projections to the striatum. Fluorescence illumination of the striatum in these brain slices reveals a dense network of YFP-positive fibres (Fig. 2*B*). We observed a difference between the CL and Pf injected animals. Whereas the entire dorsal striatum had strong expression of YFP-positive fibres in CL-injected animals (Supplemental Fig. S2*A* and *B*), the distribution was more patchy in Pf-injected animals (Supplemental Fig. S2*C* and *D*). This is likely to reflect the different patterns of arbourization of the axons of CL and Pf neurons in the striatum (Lacey *et al.* 2007), but could also be the result of partial transfection of the Pf nucleus due to its larger size (see Fig. 1*C* and *D*). We also observed YFP-positive fibres in the cortex as a consequence of the expression of ChR2-YFP in the thalamic axonal projections to the cortex (Krettek & Price, 1977; Herkenham, 1979; Groenewegen, 1988). Whole-cell, voltage-clamp and current-clamp recordings of dorsal striatal MSNs were performed while activating thalamic afferents by illuminating the striatum with brief light pulses (470 nm; 3 ms duration), as well as cortical afferents by electrical stimulation in the external capsule (Fig. 2*A*). All the experiments were performed in the presence of the $GABA_A$-receptor antagonist SR95331 (10 μm) and the $GABA_B$-receptor antagonist CGP52432 (2 μm) and at a recording temperature of 32°C. The subtype of MSN was confirmed *post hoc* by immunolabelling for preproenkephalin (PPE) which is selectively expressed by indirect pathway MSNs (Gerfen *et al.* 1990) (Fig. 2*C* and

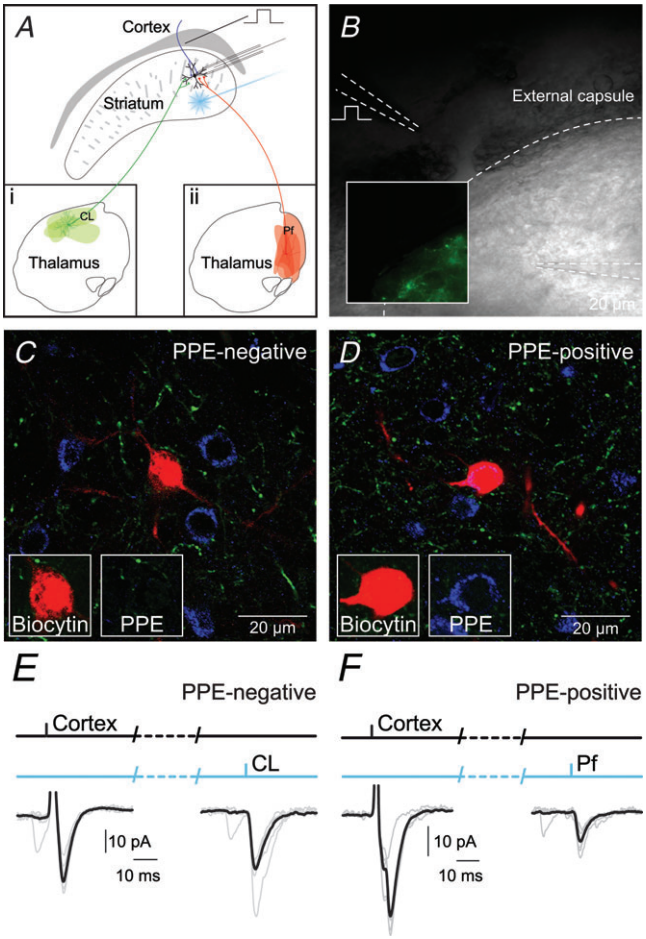

Figure 2. The majority of MSNs receive both thalamic and cortical input
A, diagram of the experimental setup for optical activation of either CL (*a*) or Pf (*b*) thalamic afferents and electrical activation of cortical afferents together with whole-cell patch-clamp recordings of MSNs. *B*, infrared differential interference contrast image of section with inset depicting fluorescence image of same region showing the YFP-expressing thalamic fibres originating from CL. *C*, confocal image of an MSN recorded and labelled with biocytin that was PPE-immunonegative and thus classified as a direct pathway MSN. *D*, confocal image of an MSN recorded and labelled with biocytin that was PPE-immunopositive and classified as an indirect pathway MSN. *E*, response of the PPE-immunonegative MSN to electrical stimulation of the cortex and optical stimulation thalamic afferents from CL. *F*, example response of a PPE-immunopositive MSN to electrical stimulation of the cortex and optical stimulation thalamic afferents from from Pf.

ChR2-YFP. *B*, diagram of a sagittal section of the mouse brain indicating where small injections were made i.e. the rostral portion (mostly CL, green) and caudal portion (mostly Pf, red) of the thalamic intralaminar nuclei. *C* and *D*, coronal sections (rostral to caudal from top to bottom) of the right hemisphere of injected CAMKII-cre mice, which were injected in either the rostral CL (*C*) or caudal Pf (*D*) thalamic nucleus. Note that the sections shown for the CL injection start more rostral than those for the PF injection. Infected neurons express YFP (green). Sections have been stained with Nissl-Cy5 to facilitate anatomical characterization (blue). DG: dentate gyrus, LV: lateral ventricle, CA3: CA3 field of the hippocampus: fr: fasciculus retroflexus, mt: mammillothalamic tract, Mhb: medial habenula, Lhb: lateral habenula.

Table 1. Basic synaptic properties of CL and Pf synapses

	CL			Pf		
	Total	PPE−	PPE+	Total	PPE−	PPE+
Voltage clamp						
Amplitude (pA)	68.8 ± 13.1*	104.3 ± 29.5*	40.8 ± 8.6*	30.7 ± 4.1*	28.7 ± 9.3	28.7 ± 4.9
Duration (ms)	19.4 ± 1.9	17.9 ± 2.2	21.9 ± 4.0	19.0 ± 1.6	17.3 ± 0.9	20.6 ± 3.4
Rise time (ms)	2.4 ± 0.4	2.2 ± 0.4	2.9 ± 0.8	2.4 ± 0.1	2.4 ± 0.3	2.5 ± 0.2
Decay time (ms)	7.3 ± 0.6	6.7 ± 0.8	8.1 ± 1.3	6.4 ± 0.2	6.2 ± 0.3	6.3 ± 0.3
LED Stimulation strength (mW)	44.9 ± 15.2	22.2 ± 4.7	68.6 ± 35.7	98.0 ± 22.5	149.8 ± 61.0	86.0 ± 31.8
Current clamp						
Amplitude (mV)	4.0 ± 0.3*	4.8 ± 0.8*	3.0 ± 0.4*	0.8 ± 0.1*	0.5 ± 0.1	0.6 ± 0.1
Duration (ms)	58.0 ± 2.4	55.3 ± 5.5	57.7 ± 5.0	49.4 ± 3.7	45.7 ± 7.2	57.7 ± 10.0
Rise time (ms)	4.7 ± 0.3	4.1 ± 0.5	4.9 ± 0.7	5.9 ± 0.4	5.8 ± 0.8	6.1 ± 0.2
Decay time (ms)	24.4 ± 1.1	23.6 ± 2.5	24.0 ± 2.1	18.3 ± 1.4	17.2 ± 3.2	19.8 ± 3.1
LED Stimulation strength (mW)	51.6 ± 10.9	52.4 ± 19.4	84.4 ± 35.6	69.8 ± 18.0	50.8 ± 11.5	81.7 ± 40.1
Paired pulse ratio	1.1 ± 0.1*	1.0 ± 0.1	1.1 ± 0.1	0.8 ± 0.1*	0.9 ± 0.2	0.9 ± 0.1
NMDA/AMPA ratio	0.8 ± 0.1*	0.7 ± 0.2	0.7 ± 0.1	2.7 ± 0.6**	2.1 ± 0.7	2.9 ± 0.8

Note: Total data includes all recorded neurons. PPE− and PPE+ groups excludes any unclassified neurons. *$P < 0.05$ and **$P < 0.01$.

D). If a recorded neuron was negative for PPE and was defined as an MSN on the basis of the somatodendritic morphology, it was considered a direct pathway MSN. A total of 117 MSNs were recorded, of which 35 (30%) were unequivocally identified as PPE-immunonegative (PPE–) and 37 (32%) as PPE-immunopositive (PPE+). Cortical and thalamic responses were observed in both PPE– and PPE+ MSNs (Fig. 2*E* and *F*).

Basic synaptic properties of thalamic synapses on MSNs

We first set out to study the minimal optical stimulation strength necessary to elicit a thalamic response in approximately half of the stimulations. We found that with LED stimulation strength as low as ∼3.5 mW, corresponding to ∼0.1 mW at the tissue, we could elicit responses in striatal MSNs from both CL and Pf afferents when recording in whole-cell, voltage-clamp mode. We found that the EPSC properties for CL and Pf synapses, using this stimulation strength, are remarkably similar, with some small differences in that CL EPSCs were larger in amplitude (CL: 18.1 ± 3.5 pA and Pf: 9.1 ± 1.3 pA; $P < 0.05$; independent samples *t* test; $n = 19$ and $n = 12$) and Pf EPSCs slightly longer in duration (CL: 27.3 ± 2.3 ms and Pf: 35.0 ± 3.8 ms; $P < 0.05$; independent samples *t* test; $n = 19$ and $n = 12$). In all subsequent experiments we used higher stimulation strength to elicit approximately half maximum amplitude responses. The average amplitude of responses following CL axon stimulation was 66.3 ± 13.5 pA (stimulation strength: 45 mW at LED/0.4 mW at tissue; $n = 16$), whereas those following Pf axon stimulation were significantly smaller at 30.7 ± 4.1 pA (stimulation strength: 98 mW at LED/0.9 mW at tissue; $P < 0.05$; independent samples *t* test; $n = 20$). The remaining EPSC characteristics (duration, rise time and decay time) were not significantly different between CL and Pf inputs (Table 1).

We further characterized the properties of EPSCs elicited by photoactivation of CL or Pf afferents by defining the postsynaptic MSN as a direct or indirect pathway neuron by PPE immunolabelling. This analysis revealed that the response to CL axon stimulation was consistently larger in amplitude than the response to Pf for both direct and indirect pathway MSNs (direct pathway: CL, 104.3 ± 33.8 pA *vs.* Pf, 28.7 ± 9.3 pA; $P < 0.05$; independent samples *t* test; both $n = 5$, and indirect pathway: CL, 40.8 ± 8.6 pA *vs.* Pf, 28.7 ± 8.6 pA; $n = 7$ and $n = 9$; Table 1). Furthermore, the analysis revealed that the response to CL axon stimulation was significantly larger in amplitude on direct pathway neurons ($P < 0.05$; independent samples *t* test; Table 1). Recordings performed in whole-cell current-clamp mode revealed a similar picture with an average amplitude of responses following CL axon stimulation of 4.0 ± 0.3 mV (stimulation strength: 52 mW at LED/0.5 mW at tissue; $n = 40$), whereas those following Pf axon stimulation were significantly smaller at 0.8 ± 0.1 mV (stimulation strength: 70 mW at LED/0.6 mW at tissue; $P < 0.05$; independent samples *t* test; $n = 25$). The response to CL axon stimulation was also consistently larger in amplitude than the response to Pf axon stimulation for both direct and indirect pathway MSNs (both $P < 0.05$; independent samples *t* test; $n = 12$ and $n = 6$, and $n = 10$ and $n = 6$; Table 1). Lastly, the analysis revealed that the response to CL axon stimulation

was again significantly larger in amplitude on direct pathway neurons ($P < 0.05$; independent samples t test; Table 1). The responses obtained with LED stimulation are likely to be a consequence of the stimulation of multiple axons rendering the interpretation of different peak amplitudes of the responses uncertain. In order to facilitate the isolation of single axons and obtain a measure of the amplitude of an unitary response the experiment was repeated in whole-cell, voltage-clamp mode in which afferents were activated using 473 nm laser stimulation (100 mW maximum output) with a 10 μm spot diameter (Supplemental Fig. S3*A*). Initially, the stimulation intensity was moderate, 50% of maximum output at the laser, corresponding to 0.13 mW at the tissue, to aid in the detection of connections between fibres and MSNs. When an EPSC was observed, the stimulation intensity was reduced until only failures could be observed. The stimulation intensity was then incrementally changed with 5% step increases in laser output power until all stimulations led to a successful EPSC as measured from the postsynaptic neuron. Responses were accepted as unitary if the amplitude remained constant over a range where failures dropped. Averaging the responses within this range (100% failures – 0% failures) revealed that EPSCs for the CL synapses were significantly larger than for the Pf synapses (CL: 38 ± 10.3 pA and Pf: 14.7 ± 1.6 pA; $P < 0.05$; independent samples t test; $n = 25$ and $n = 33$; Supplemental Fig. S3*B* and *C*). Similar amplitude responses could also be seen occurring spontaneously during the recordings.

These results suggest, first, that thalamic inputs from CL produce a larger depolarization of both direct and indirect pathway MSNs than Pf inputs. Secondly, CL inputs to direct pathway MSNs produce a stronger response than those to indirect pathway MSNs.

Short-term plastic properties of thalamic and cortical synapses on MSNs

We next set out to investigate the dynamic properties of the excitatory synapses from CL, Pf and cortex. MSNs were recorded in whole-cell, voltage-clamp and current-clamp mode while thalamic and cortical afferents were activated using a paired-pulse stimulation protocol consisting of two pulses at 50 ms interval. We found that the paired-pulse ratio (PPR) for afferents from CL are facilitating (mean ratio of S2/S1: 1.11 ± 0.05; $P < 0.05$; one sample t test; $n = 56$), whereas those from Pf are depressing (mean ratio of S2/S1: 0.80 ± 0.08; $P < 0.05$; one sample t test; $n = 22$). The variation in paired-pulse ratio between individual MSNs leads to an average 'neutral' PPR in the case of cortical afferents (mean ratio of S2/S1: 1.00 ± 0.04; $n = 54$; Fig. 3*A*). We did not observe any differences in the PPR of CL, Pf and cortical synapses between direct pathway and indirect pathway MSNs (Table 1).

Next, we investigated the dynamics of these inputs during longer trains of stimulation at 5 Hz, 10 Hz and 20 Hz. These analyses revealed a similar picture to that seen during paired-pulse stimulation. Firstly, whereas all responses significantly depress eventually, only the responses of CL inputs are facilitating for the first few spikes during both 10 and 20 Hz stimulation (one sample t test; both $P < 0.05$; $n = 33$ and $n = 46$; Fig. 3*B*). Secondly, the depressing cortical response recovers more quickly than the combined thalamic responses after both 10 Hz and 20 Hz stimulation (10 Hz: cortical 0.87 ± 0.05 *vs.* thalamic 0.57 ± 0.05 and 20 Hz: cortical 0.90 ± 0.12 *vs.* thalamic 0.60 ± 0.05; $P < 0.01$ and $P < 0.05$; both independent samples t test; $n = 20$ and 48 and $n = 28$ and 62). Lastly, the Pf response is significantly depressing following both 10 and 20 Hz train stimulation (one-sample t test; $P < 0.05$; $n = 15$ and 16) and the rate of recovery was the least of all three responses (Fig. 3*B*). The recovery time constant of ChR2 is relatively long (>50 ms) and the channels desensitize when repeatedly activated (Petreanu *et al.* 2007; Zhang & Oertner, 2007; Cruikshank *et al.* 2010), which would suggest that the PPR we observe at these synapses are underestimates of the true PPR. Indeed, when we measured the PPR of corticostriatal synapses using optical stimulation of cortical afferents, we found that it is lower than when measured following electrical stimulation (optical: 0.73 ± 0.12 *vs.* electrical: 1.00 ± 0.04; $P < 0.05$; independent samples t test; $n = 11$ and $n = 54$). We attempted to circumvent this problem, and study the dynamic properties of the thalamic synapses at higher frequencies, by using the light activatable channel ChETA, which exhibits less desensitization and is able to follow higher frequencies of stimulation (>50 Hz) (Gunaydin *et al.* 2010). However, we were not able to elicit reliable responses from slices taken from CL-injected animals, despite the presence of YFP-positive fibres within the striatum (4 animals; 15 putative MSNs). In all subsequent experiments only ChR2 was used.

In conclusion, with the caveat that all optically derived PPRs are likely to be underestimates, the dynamic properties of CL, Pf and cortical synapses differ in that CL synapses are facilitating suggesting that they are well-suited to drive MSN depolarization during trains or bursts of action potentials whereas Pf and cortical synapses are largely depressing.

Dominant ionotropic glutamate receptors at thalamic and cortical synapses

We found differences in the short-term dynamics, as well as the amplitude of postsynaptic responses, but to what extent these are the result of differential expression of

postsynaptic receptors is unknown. We therefore investigated the ionotropic glutamate receptor composition postsynaptic to CL, Pf and cortical synapses. Stimulated excitatory events were recorded from MSNs in whole-cell voltage-clamp mode at a holding potential of +40 mV and recorded events consisted of combined NMDA and AMPA receptor-mediated currents (Fig. 4*A*). After baseline recording, D-AP5 (50 μm) was bath applied to block the NMDA receptor-mediated currents, thereby isolating the AMPA receptor-mediated component. Analysis of the ratio of peak amplitude currents showed that CL synapses are dominated by AMPA receptor-mediated currents, whereas Pf synapses are dominated by NMDA receptor-mediated currents (mean NMDA/AMPA ratio for CL: 0.78 ± 0.09; $P < 0.05$ and Pf: 2.66 ± 0.56; $P < 0.01$; both one sample t test; $n = 20$ and $n = 12$; Fig. 4*B*). Cortical synapses exhibit an NMDA/AMPA ratio in-between those of CL and Pf synapses, but are dominated by NMDA receptor-mediated currents (mean NMDA/AMPA ratio for cortical, peak amplitude: 1.60 ± 0.27; $P < 0.05$; one sample t test; $n = 14$; Fig. 4*B*). These results suggest that inputs from CL are very efficient at depolarizing MSNs, whereas inputs from Pf would have little effect on MSNs, at resting membrane potentials.

Long-term plasticity at Pf, but not CL, synapses

The large NMDA/AMPA ratio suggests that NMDA receptors gate the dominant excitatory postsynaptic current at Pf synapses. This would enable this synapse to gate substantial amounts of Ca^{2+} if appropriately

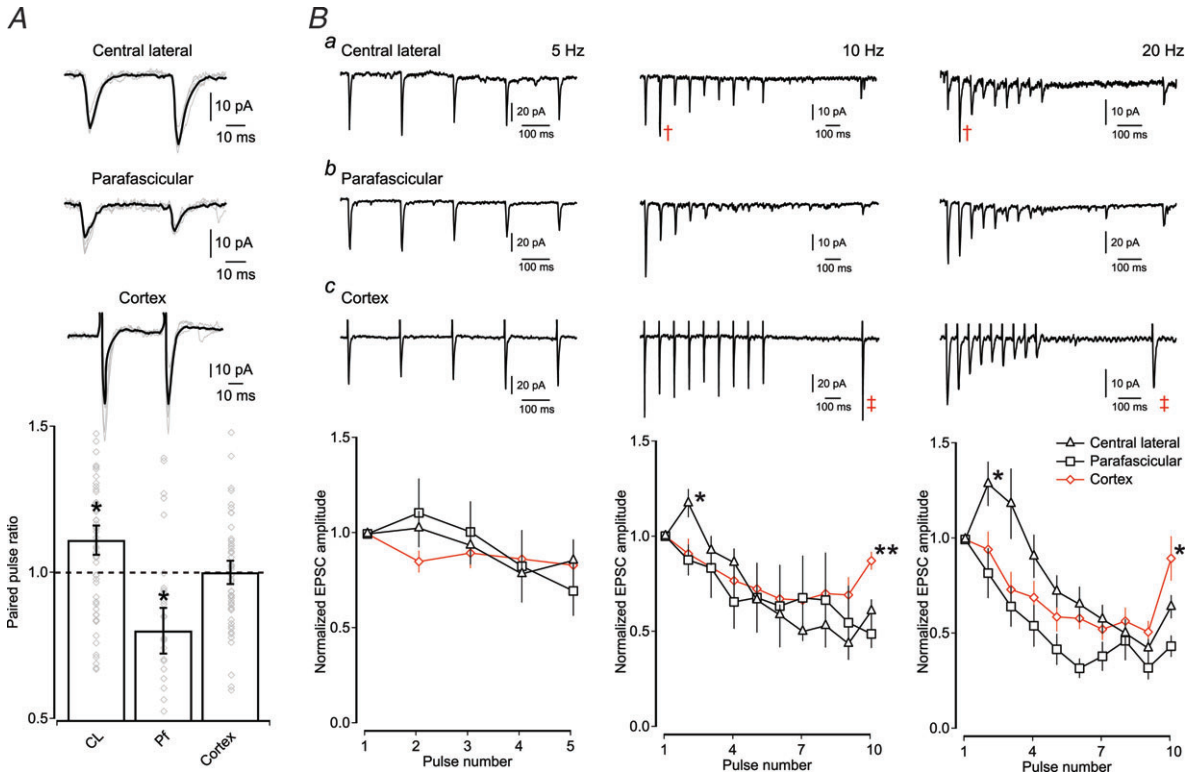

Figure 3. Dynamic properties of CL, Pf and cortical synapses on MSNs
A, top, example traces of paired-pulse responses of CL, Pf and cortical synapses on MSNs (grey traces; responses to optical and electrical single paired-pulse stimulations and superimposed black trace; average response to paired-pulse stimulations for a MSN). Note that each excitatory input has a distinct PPR. Bottom, bar plot of average PPR (mean ± SEM) showing that CL synapses are significantly facilitating ($P < 0.05$; $n = 56$), Pf synapses are significantly depressing ($P < 0.05$; $n = 22$), whereas the average PPR of cortical synapses is neutral ($P > 0.05$; $n = 54$). Diamond symbols in the bar plot indicate the average PPR of individual neurons. *B*, short-term dynamics of responses when excitatory afferents from CL (*a*), Pf (*b*) and cortical (*c*) synapses onto MSNs are stimulated at 5 Hz, 10 Hz and 20 Hz. Top, example traces are given for each afferent at each frequency. Note the facilitating response at CL synapses at 10 Hz and 20 Hz (cross symbol). Note the quick recovery of the cortical input onto MSNs (double cross symbol). Bottom, graph of average normalized EPSC amplitude (mean ± SEM) to train stimulations at 5 Hz (left), 10 Hz (middle) and 20 Hz (right). Note the lack of short-term dynamics using 5 Hz stimulation (CL; $n = 30$, Pf; $n = 12$ and cortex; $n = 22$). At stimulation frequencies of 10 and 20 Hz the CL inputs exhibit short-term facilitation ($P < 0.05$; $n = 33$ and 46), whereas those from Pf and cortex show depression from the first pulse onwards ($P < 0.05$; $n = 15$ and 16).

activated, and this could facilitate Ca^{2+}-dependent processes including some forms of synaptic plasticity. We therefore investigated the ability of CL and Pf synapses to undergo pairing-induced synaptic plasticity by performing whole-cell, patch-clamp recordings from MSNs in current-clamp mode and combining optical stimulation of thalamic afferents with postsynaptic action potentials. We recorded baseline EPSPs for 5 min, after which we used a protocol consisting of 100 repeated pairings at 1 Hz of an optically evoked thalamic EPSP followed, with a delay of approximately 8 ms, by an action potential in the MSN evoked by a suprathreshold current injection. We also performed this experiment in reverse, i.e. an action potential was initiated in the MSN by a suprathreshold current injection, followed by a delay of approximately 8 ms, by an optically evoked thalamic EPSP. We investigated the effect of both pairing protocols on the efficacy of the thalamic input. We found that these protocols lead to long-term depression of evoked EPSPs at Pf synapses (pre–post to $62.0 \pm 2.9\%$ of control and post–pre to $71.2 \pm 6.0\%$ of control; both $P < 0.05$; Wilcoxon's signed-rank test; $n = 7$ and $n = 6$; Fig. 5*B*) after either pre–post or post–pre pairing. However, the same protocols applied to CL synapses did not result in any change in the amplitude of evoked EPSPs using (pre–post to $101.0 \pm 4.1\%$ and post–pre to $96.5 \pm 4.7\%$; both $P > 0.05$; Wilcoxon's signed-rank test; $n = 5$ and $n = 5$; Fig. 5*A*).

To investigate the mechanisms underlying this plasticity we repeated both the pairing protocols for Pf synapses, but this time included either the NMDA receptor antagonist, MK-801 (1 mM), or the calcium chelator, EGTA (10 mM), in the intracellular solution. The presence of MK-801 or EGTA blocked the induction of long-term depression at Pf synapses using the pre–post protocol (Pf *vs.* Pf + MK-801: $91.1 \pm 9.6\%$; $P < 0.01$; Mann–Whitney test; $n = 7$ and $n = 7$; MK-801 only: $91.1 \pm 9.6\%$; $P > 0.05$; Wilcoxon's signed-rank test; $n = 7$ and Pf *vs.* Pf + EGTA $89.4 \pm 4.2\%$; $P < 0.01$; Mann–Whitney test; $n = 7$ and $n = 5$; EGTA only: $89.4 \pm 4.2\%$; $P > 0.05$; Wilcoxon's signed-rank test; $n = 5$; Fig. 5*C* and *D*) and post–pre protocol (MK-801 only: $90.3 \pm 6.2\%$; $P > 0.05$; Wilcoxon's signed-rank test; $n = 4$ and EGTA only: $91.4 \pm 5.8\%$; $P > 0.05$; Wilcoxon's signed-rank test; $n = 4$; Fig. 5*C* and *D*), although the comparisons between groups showed only a trend for the post–pre protocol (Pf *vs.* Pf + MK-801: $90.3 \pm 6.2\%$; $P = 0.055$; Mann–Whitney test; $n = 6$ and $n = 4$; Pf *vs.* Pf + EGTA $91.4 \pm 5.8\%$; $P = 0.055$; Mann–Whitney test; $n = 6$ and $n = 4$).

To investigate whether the observed plasticity also included a presynaptic component we compared the PPR at these synapses before and after the induction protocol. After the induction protocol the PPR at Pf synapses significantly increased (pre–post: 0.4 ± 0.1 to 1.1 ± 0.2 and post–pre: 0.7 ± 0.1 to 1.3 ± 0.1; both $P < 0.05$; paired samples *t* test; $n = 7$ and $n = 4$), whereas the same protocol did not lead to changes in the PPR at CL synapses (pre–post: 1.1 ± 0.2 to 1.2 ± 0.1; post–pre: 1.0 ± 0.1 to 0.9 ± 0.1; $P > 0.05$; paired samples *t* test; $n = 5$ and $n = 4$) or at Pf synapses in the presence of MK-801 (pre–post: 0.8 ± 0.1 to 0.6 ± 0.1 and post–pre 0.9 ± 0.1 to 0.9 ± 0.2; both $P > 0.05$; paired samples *t* test; $n = 6$ and $n = 4$) or EGTA (pre–post: 0.7 ± 0.1 to 0.6 ± 0.1 and post–pre: 0.6 ± 0.1 to 0.8 ± 0.1; both $P > 0.05$; paired samples *t* test; $n = 5$ and $n = 4$).

These results thus suggest that Pf synapses, but not CL synapses, exhibit long-term plasticity which is dependent on postsynaptic NMDA receptors and calcium entry and might also involve presynaptic changes.

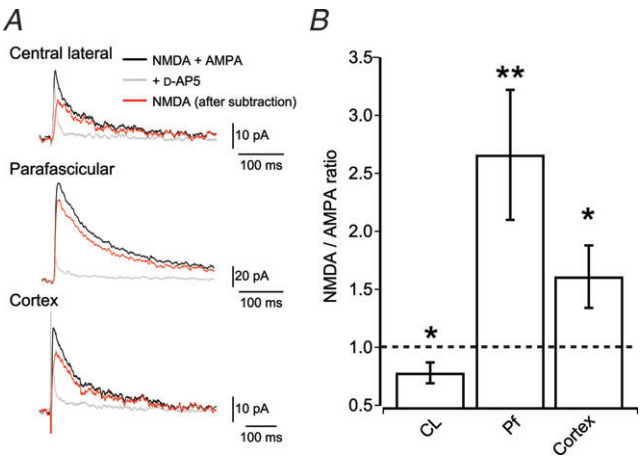

Figure 4. NMDA/AMPA receptor ratio at CL, Pf and cortical synapses on MSNs
A, example traces of postsynaptic excitatory currents recorded from MSNs held at +40 mV. The black trace shows combined AMPA receptor and NMDA receptor-mediated currents, the grey trace shows isolated AMPA receptor-mediated currents in the presence of D-AP5. Subtraction of the AMPA receptor-mediated current trace from the combined trace revealed the NMDA receptor-mediated current (red trace). *B*, bar plot of the average NMDA/AMPA ratio of CL, Pf and cortical synapses on MSNs (mean ± SEM). Note that CL synapses exhibit predominant AMPA receptor-mediated currents ($P < 0.05$; $n = 20$), whereas Pf synapses exhibit predominant NMDA receptor-mediated currents ($P < 0.01$; $n = 12$). Similarly, cortical inputs also exhibit predominant NMDA receptor-mediated currents ($P < 0.05$; $n = 14$).

Discussion

The main findings of the present study are that thalamostriatal innervation of MSNs originating in different regions of the intralaminar thalamus have markedly different properties. Using an optogenetic approach in adult mice we were able to dissociate between the rostral (CL) and caudal (Pf) intralaminar inputs to MSNs. First, we find that CL synapses give rise to larger amplitude responses than Pf synapses.

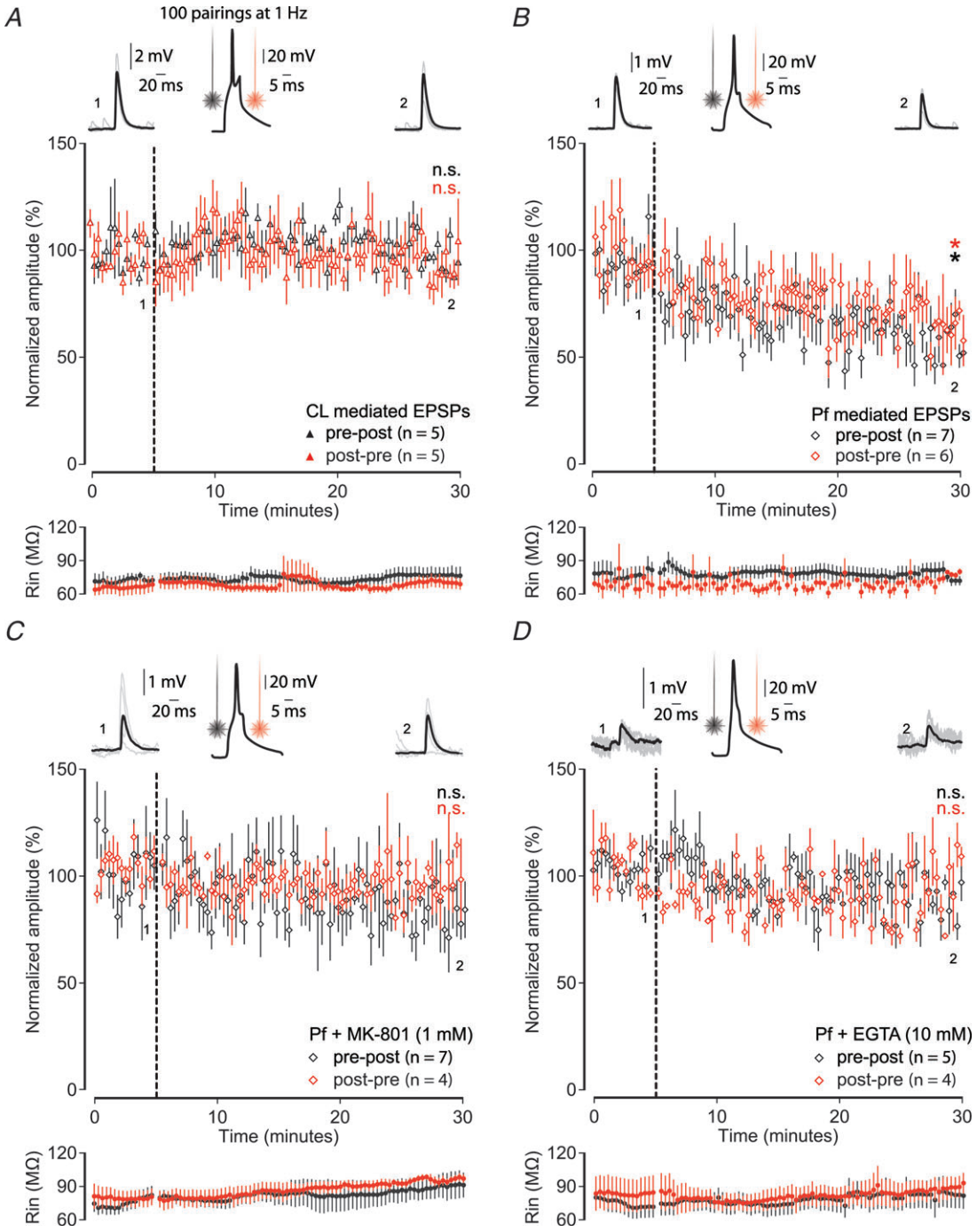

Figure 5. Long-term plasticity at Pf, but not CL, synapses
A and *B*, pairing activation of thalamic afferents with action potentials in MSNs (100 pairings at 1 Hz) leads to long-term plasticity at Pf (*B*), but not CL (*A*) synapses in both pre–post (black) and post–pre (red) pairings. Graphs display the average EPSP amplitude during a 5 min baseline and for 25 min after the pairing protocol (indicated by the black dashed line). Left and right top, individual example EPSPs before and after the pre–post pairing protocol with the numbers corresponding to time points in the graph. Middle top, an example recording of an action potential in an MSN, in response to suprathreshold current injection, with the black and red line indicating the time at which the thalamic afferents are activated. Bottom, graphs display the average input resistance during the recordings. *C* and *D*, pairing-induced plasticity was blocked by including the NMDA receptor blocker MK-801 (1 mM) (*C*) or the calcium chelator EGTA (10 mM) (*D*) in the intracellular solution.

Secondly, CL synapses are facilitating, whereas Pf synapses are depressing. Thirdly, CL synapses predominantly express postsynaptic AMPA receptors, whereas Pf synapses are predominantly associated with postsynaptic NMDA receptors. Finally, the relatively high expression of NMDA receptors at Pf synapses facilitates pairing-induced plasticity at these, but not CL, synapses. Corticostriatal synapses exhibited properties in between those of CL and Pf synapses. The observed heterogeneity in synaptic properties suggests that CL and Pf inputs subserve different roles in striatal computation.

Properties of thalamostriatal synapses on MSNs

We used optogenetic tools to isolate specific thalamic nuclei and their projections to MSNs by injections of AAV2 particles containing the double-floxed sequence for ChR2 in either the rostral or caudal portion of the intralaminar nuclei of CAMKII-cre mice. This approach led to the expression of ChR2 in excitatory thalamic neurons around the site of injection including their axonal projections to the striatum. We were thus able to selectively stimulate and dissect out the properties of CL and Pf afferents in slices of striatum, something that is not possible using conventional electrical stimulation in slices or indeed, *in vivo*. Furthermore, as we used mice at 2 to 3 months of age enabling us to investigate the properties of the thalamic synapses in an adult thalamostriatal circuit. We combined optical stimulation with electrical stimulation of cortical afferents in the external capsule to define their properties in adult animals and to compare them to thalamostriatal synapses, albeit recognizing the difficulty of comparing electrical and optical stimulation (Petreanu *et al.* 2007; Zhang & Oertner, 2007; Cruikshank *et al.* 2010). Although the CL and Pf nuclei were targeted, it cannot be excluded that neurons of neighbouring thalamic nuclei (Xu *et al.* 1991; Groenewegen & Berendse, 1994; Smith *et al.* 2004) might have also been recruited, nor can we exclude with certainty that there was not cross-contamination between the CL and Pf nuclei. With the ongoing development of specific mouse cre recombinase lines it may be possible in the future to more easily isolate and selectively activate these nuclei and other inputs. Using this optogenetic approach we demonstrated that MSNs giving rise to the direct pathway and those giving rise to the indirect pathway (identified by PPE immunoreactivity) both receive input from Pf or CL. Furthermore, concurrent electrical stimulation of cortical afferents revealed that MSNs that responded to stimulation of thalamic fibres also receive input from the cortex. Previous electrophysiological (Kitai *et al.* 1976; Ding *et al.* 2010) and anatomical studies (Doig *et al.* 2010) have shown convergence of cortical and thalamic input at the level of individual MSNs, the present results now further demonstrate that individual direct and indirect pathway MSNs receiving cortical input may also receive input from CL or Pf. Many previous studies (Day *et al.* 2006; Wang *et al.* 2006; Kreitzer & Malenka, 2007; Ade *et al.* 2008; Cepeda *et al.* 2008; Andre *et al.* 2010) have benefited from the generation of the D1- and D2-GFP BAC transgenic mouse lines (Gong *et al.* 2003) which express GFP under the D1 or D2 receptor promoter to facilitate the distinction between the two main types of striatal projection neuron. However, recent studies have suggested that homozygous D2-GFP mice exhibit abnormal physiology and behaviour (Kramer *et al.* 2011), and although the background strain of mice (Chan *et al.* 2012) and zygosity state (Nelson *et al.* 2012) are important factors, even the heterozygous transgenic mice have been shown to exhibit an altered physiology (Bagetta *et al.* 2011). All this suggests that future studies could benefit from using *post hoc* immunohistochemistry against dopamine receptor subtypes (Bagetta *et al.* 2011) or intracellular markers, such as used in this study, to distinguish between the two main populations of striatal MSN.

Analysis of the basic synaptic properties of CL and Pf inputs showed that stimulation of CL afferents led to larger amplitude postsynaptic responses than stimulation of Pf afferents, and especially so for the direct pathway neurons. CL inputs might make more synapses on individual MSNs than Pf inputs, but it is currently unknown if this and/or differences in release probability, location of synaptic contacts or density of postsynaptic receptors is responsible. The short-term dynamic responses of the synapses revealed by paired-pulse and train stimulation further emphasized the different properties of CL and Pf synapses. Stimulation at 5 Hz did not lead to changed dynamics and stimulation at higher frequencies led all three excitatory inputs (CL, Pf and cortical) to eventually depress. However, CL synapses exhibited a prominent short-term facilitation prior to depression. This was even more prominent during 20 Hz stimulation; while Pf and cortical synapses depress with every subsequent spike, CL synapses are facilitated for the first few spikes. However, it cannot be excluded that, despite using the same construct with the same promoter, the level of expression may be different between neurons in the two nuclei, with higher levels of expression diminishing the sensitivity to desensitization. This, together with the fact that the ChR2 construct is prone to desensitization, suggests that our observations may be underestimates of the short-term dynamics of these synapses. Furthermore, it is important to keep in mind that the physiological consequences of train stimulation may differ *in situ* with intact synaptic inhibition, as the temporal window for integration of excitatory inputs is often under the control of feed-forward inhibition (Gabernet *et al.* 2005). This might explain the results of previous studies showing short-term depression (Ding *et al.* 2008) or facilitation

(Smeal *et al.* 2007) of thalamostriatal synapses in mouse and rat respectively. Moreover, in these studies the thalamostriatal pathways were examined as a single entity using electrical stimulation and could also result from a preferential activation of sub-sets of afferents, depending on electrode placement. Since CL neurons give rise to LTS bursts that can reach a firing frequency of up to 250 Hz *in vivo* (Lacey *et al.* 2007), it is critical to know whether similar dynamics hold true at this spike frequency. We attempted to investigate this using ChETA, a light-activated channel that can respond to much higher stimulation frequencies than ChR2 (Gunaydin *et al.* 2010). However, we did not get reliable responses during optical stimulation, suggesting the single channel conductance (Berndt *et al.* 2011) or expression of the channel, although sufficient for somatic activation, might be too low to elicit reliable transmitter release directly from axons. Nevertheless, our data, together with the observation that CL synapses predominantly express AMPA receptors, suggest that small bursts of action potentials arriving from CL would be faithfully transmitted and are likely to be very efficient at depolarizing MSNs. In contrast to CL synapses, Pf synapses exhibit short-term depression and mainly express postsynaptic NMDA receptors, suggesting that these synapses do not lead to strong depolarization of MSNs at resting membrane potential when NMDA receptors are blocked by Mg^{2+}. However, the expression of postsynaptic NMDA receptors may lead to sufficient Ca^{2+} influx, under the right conditions, to facilitate Ca^{2+}-dependent processes, including state transitions (Plotkin *et al.* 2011), local dendritic spike modulation (Losonczy *et al.* 2008) or synaptic plasticity (Kreitzer & Malenka, 2008). As MSNs have been shown to express calcium-permeable, GluA1 subunit-containing, AMPA receptors (Bernard *et al.* 1997; Gotz *et al.* 1997) it cannot be excluded that CL synapses could also generate a Ca^{2+} influx under certain conditions (Carter & Sabatini, 2004).

We found that the properties of cortical synapses in the adult striatum lie in between those of CL and Pf synapses. Electrical stimulation of the external capsule leads to large amplitude responses in both direct and indirect pathway MSNs. The paired-pulse and train stimulation experiments showed that cortical synapses are mostly depressing, consistent with previous studies (Smeal *et al.* 2007). We did not find the brief facilitation seen in slices from younger animals (Ding *et al.* 2008; Ellender *et al.* 2011), suggesting this might be an age-dependent phenomenon. Although we have previously shown that the properties of corticostriatal synapses in striatal slices of young mice are similar whether examined by electrical or optical stimulation at low frequencies (Ellender *et al.* 2011), it is important to be cautious when comparing electrical and optical stimulation at these higher frequencies as ChR2 has been shown to desensitize with repeated stimulation (Zhang & Oertner, 2007; Cruikshank *et al.* 2010). Indeed, we find a lower paired-pulse ratio of corticostriatal synapses using optical stimulation. Lastly, we found that cortical synapses on MSNs express a high proportion of NMDA receptors, as previously shown by Smeal *et al.* (2008), (but see Kreitzer & Malenka, 2007; Ding *et al.* 2008). Our data thus suggest that of all excitatory synapses on MSNs, those from the CL are likely to be the most effective in the depolarizing control of MSN firing, those from Pf are likely to be responsible for most of the Ca^{2+} influx, whereas those from the cortex are likely to contribute to both aspects.

Plasticity at thalamostriatal synapses

Synaptic plasticity at excitatory synapses in the striatum is complicated; both LTD and LTP have been reported and are variously dependent on the presence of neuromodulators, frequency of stimulation and/or pairing with postsynaptic action potentials (Mahon *et al.* 2004; Calabresi *et al.* 2007; Surmeier *et al.* 2007; Kreitzer & Malenka, 2008). We found that pairing optical stimulation of thalamic synapses together with postsynaptic action potentials in MSNs leads to long-term depression at Pf, but not CL synapses in both pre–post and post–pre pairing protocols. This plasticity is blocked if the calcium chelator, EGTA, or the NMDA receptor antagonist, MK-801, is included in the intracellular solution, suggesting that the plasticity is dependent on calcium influx through postsynaptic NMDA receptors. However, as the observed plasticity at Pf synapses was associated with a concomitant change in the paired-pulse ratio it might well also have a presynaptic component (Kreitzer & Malenka, 2005, 2007). Similar pairing-induced long-term depression has been observed at corticostriatal synapses (Fino *et al.* 2005; Pawlak & Kerr, 2008; Shindou *et al.* 2011), but in these studies the spike order determined the sign of plasticity (long-term potentiation *vs.* long-term depression). In our study both pre–post and post–pre pairing led to long-term depression at Pf synapses. The inability to observe other forms of long-term plasticity at Pf, and possibly CL synapses, might well be the result of washout of intracellular factors during whole-cell patch-clamp recordings, be dependent on different induction protocols (e.g. high-frequencies of stimulation) or due to an artificially elevated release probability in ChR2 transfected fibres. The sign of plasticity at corticostriatal synapses seemed to be dependent also on the state of inhibitory GABAergic transmission (Fino *et al.* 2010). Furthermore, it has been shown that dopaminergic tone can modulate plasticity (Wang *et al.* 2006) and bidirectional spike timing-dependent plasticity at glutamatergic synapses on MSNs (Shen *et al.* 2008). In the latter study the glutamatergic synapses were stimulated locally, within the striatum, and it may well be that some of their observations are the result of

recruitment of thalamic synapses. These studies suggest that thalamostriatal plasticity might well be regulated by inhibitory GABAergic transmission and the presence of certain neuromodulators, including dopamine (Pawlak & Kerr, 2008), serotonin (Mathur *et al.* 2011), histamine (Ellender *et al.* 2011), endocannabinoids (Kreitzer & Malenka, 2007) and others (Blomeley & Bracci, 2008). In particular, a role for cholinergic interneurons cannot be excluded (Lapper & Bolam, 1992; Ding *et al.* 2010), as Pf synapses have been shown to activate cholinergic interneurons strongly (Ding *et al.* 2010; Threlfell *et al.* 2012), and whose activity can subsequently modulate the release of dopamine directly at dopaminergic terminals (Cachope *et al.* 2012; Threlfell *et al.* 2012) producing a potentially complex interplay between neuromodulation and synaptic plasticity. Lastly, it should be noted that the calcium inflow at Pf synapses might also modulate the induction of plasticity at other synapses on MSNs (Popescu *et al.* 2007) or, depending on location of the synapse (spine *vs.* dendrite), may initiate local dendritic spikes that facilitate cooperative plasticity (Golding *et al.* 2002).

In conclusion, the present study shows that the thalamostriatal synapses from neurons in the rostral and caudal intralaminar nuclei exhibit a hitherto unrecognized heterogeneity, suggesting a differential contribution to information processing in the striatum. Our findings of the properties of CL and Pf synapses are reminiscent of the proposal that thalamic neurons can fulfill the role of 'drivers' or 'modulators' (Sherman & Guillery, 1998; Lee & Sherman, 2011), suggesting that CL synapses may act as drivers of MSN spiking activity whereas Pf synapses may subserve the role of modulators of the activity of MSNs.

References

Ade KK, Janssen MJ, Ortinski PI & Vicini S (2008). Differential tonic GABA conductances in striatal medium spiny neurons. *J Neurosci* **28**, 1185–1197.

Andre VM, Cepeda C, Cummings DM, Jocoy EL, Fisher YE, William Yang X & Levine MS (2010). Dopamine modulation of excitatory currents in the striatum is dictated by the expression of D1 or D2 receptors and modified by endocannabinoids. *Eur J Neurosci* **31**, 14–28.

Bagetta V, Picconi B, Marinucci S, Sgobio C, Pendolino V, Ghiglieri V, Fusco FR, Giampa C & Calabresi P (2011). Dopamine-dependent long-term depression is expressed in striatal spiny neurons of both direct and indirect pathways: implications for Parkinson's disease. *J Neurosci* **31**, 12513–12522.

Berendse HW & Groenewegen HJ (1990). Organization of the thalamostriatal projections in the rat, with special emphasis on the ventral striatum. *J Comp Neurol* **299**, 187–228.

Bernard V, Somogyi P & Bolam JP (1997). Cellular, subcellular, and subsynaptic distribution of AMPA-type glutamate receptor subunits in the neostriatum of the rat. *J Neurosci* **17**, 819–833.

Berndt A, Schoenenberger P, Mattis J, Tye KM, Deisseroth K, Hegemann P & Oertner TG (2011). High-efficiency channelrhodopsins for fast neuronal stimulation at low light levels. *Proc Natl Acad Sci U S A* **108**, 7595–7600.

Blomeley C & Bracci E (2008). Substance P depolarizes striatal projection neurons and facilitates their glutamatergic inputs. *J Physiol* **586**, 2143–2155.

Boyden ES, Zhang F, Bamberg E, Nagel G & Deisseroth K (2005). Millisecond-timescale, genetically targeted optical control of neural activity. *Nat Neurosci* **8**, 1263–1268.

Buchwald NA, Price DD, Vernon L & Hull CD (1973). Caudate intracellular response to thalamic and cortical inputs. *Exp Neurol* **38**, 311–323.

Burger C, Gorbatyuk OS, Velardo MJ, Peden CS, Williams P, Zolotukhin S, Reier PJ, Mandel RJ & Muzyczka N (2004). Recombinant AAV viral vectors pseudotyped with viral capsids from serotypes 1, 2, and 5 display differential efficiency and cell tropism after delivery to different regions of the central nervous system. *Mol Ther* **10**, 302–317.

Cachope R, Mateo Y, Mathur BN, Irving J, Wang HL, Morales M, Lovinger DM & Cheer JF (2012). Selective activation of cholinergic interneurons enhances accumbal phasic dopamine release: setting the tone for reward processing. *Cell Rep* **2**, 33–41.

Calabresi P, Picconi B, Tozzi A & Di Filippo M (2007). Dopamine-mediated regulation of corticostriatal synaptic plasticity. *Trends Neurosci* **30**, 211–219.

Cardin JA, Carlen M, Meletis K, Knoblich U, Zhang F, Deisseroth K, Tsai LH & Moore CI (2009). Driving fast-spiking cells induces gamma rhythm and controls sensory responses. *Nature* **459**, 663–667.

Carter AG & Sabatini BL (2004). State-dependent calcium signaling in dendritic spines of striatal medium spiny neurons. *Neuron* **44**, 483–493.

Castle M, Aymerich MS, Sanchez-Escobar C, Gonzalo N, Obeso JA & Lanciego JL (2005). Thalamic innervation of the direct and indirect basal ganglia pathways in the rat: Ipsi- and contralateral projections. *J Comp Neurol* **483**, 143–153.

Cepeda C, Andre VM, Yamazaki I, Wu N, Kleiman-Weiner M & Levine MS (2008). Differential electrophysiological properties of dopamine D1 and D2 receptor-containing striatal medium-sized spiny neurons. *Eur J Neurosci* **27**, 671–682.

Chan CS, Peterson JD, Gertler TS, Glajch KE, Quintana RE, Cui Q, Sebel LE, Plotkin JL, Shen W, Heiman M, Heintz N, Greengard P & Surmeier DJ (2012). Strain-specific regulation of striatal phenotype in Drd2-eGFP BAC transgenic mice. *J Neurosci* **32**, 9124–9132.

Cruikshank SJ, Urabe H, Nurmikko AV & Connors BW (2010). Pathway-specific feedforward circuits between thalamus and neocortex revealed by selective optical stimulation of axons. *Neuron* **65**, 230–245.

Day M, Wang Z, Ding J, An X, Ingham CA, Shering AF, Wokosin D, Ilijic E, Sun Z, Sampson AR, Mugnaini E, Deutch AY, Sesack SR, Arbuthnott GW & Surmeier DJ (2006). Selective elimination of glutamatergic synapses on striatopallidal neurons in Parkinson disease models. *Nat Neurosci* **9**, 251–259.

Ding J, Peterson JD & Surmeier DJ (2008). Corticostriatal and thalamostriatal synapses have distinctive properties. *J Neurosci* **28**, 6483–6492.

Ding JB, Guzman JN, Peterson JD, Goldberg JA & Surmeier DJ (2010). Thalamic gating of corticostriatal signaling by cholinergic interneurons. *Neuron* **67**, 294–307.

Doig NM, Moss J & Bolam JP (2010). Cortical and thalamic innervation of direct and indirect pathway medium-sized spiny neurons in mouse striatum. *J Neurosci* **30**, 14610–14618.

Ellender TJ, Huerta-Ocampo I, Deisseroth K, Capogna M & Bolam JP (2011). Differential modulation of excitatory and inhibitory striatal synaptic transmission by histamine. *J Neurosci* **31**, 15340–15351.

Fino E, Glowinski J & Venance L (2005). Bidirectional activity-dependent plasticity at corticostriatal synapses. *J Neurosci* **25**, 11279–11287.

Fino E, Paille V, Cui Y, Morera-Herreras T, Deniau JM & Venance L (2010). Distinct coincidence detectors govern the corticostriatal spike timing-dependent plasticity. *J Physiol* **588**, 3045–3062.

Fujiyama F, Unzai T, Nakamura K, Nomura S & Kaneko T (2006). Difference in organization of corticostriatal and thalamostriatal synapses between patch and matrix compartments of rat neostriatum. *Eur J Neurosci* **24**, 2813–2824.

Gabernet L, Jadhav SP, Feldman DE, Carandini M & Scanziani M (2005). Somatosensory integration controlled by dynamic thalamocortical feed-forward inhibition. *Neuron* **48**, 315–327.

Gerfen CR, Engber TM, Mahan LC, Susel Z, Chase TN, Monsma FJ Jr & Sibley DR (1990). D1 and D2 dopamine receptor-regulated gene expression of striatonigral and striatopallidal neurons. *Science* **250**, 1429–1432.

Golding NL, Staff NP & Spruston N (2002). Dendritic spikes as a mechanism for cooperative long-term potentiation. *Nature* **418**, 326–331.

Gong S, Zheng C, Doughty ML, Losos K, Didkovsky N, Schambra UB, Nowak NJ, Joyner A, Leblanc G, Hatten ME & Heintz N (2003). A gene expression atlas of the central nervous system based on bacterial artificial chromosomes. *Nature* **425**, 917–925.

Gotz T, Kraushaar U, Geiger J, Lubke J, Berger T & Jonas P (1997). Functional properties of AMPA and NMDA receptors expressed in identified types of basal ganglia neurons. *J Neurosci* **17**, 204–215.

Graybiel AM, Aosaki T, Flaherty AW & Kimura M (1994). The basal ganglia and adaptive motor control. *Science* **265**, 1826–1831.

Grillner S, Hellgren J, Menard A, Saitoh K & Wikstrom MA (2005). Mechanisms for selection of basic motor programs–roles for the striatum and pallidum. *Trends Neurosci* **28**, 364–370.

Groenewegen HJ (1988). Organization of the afferent connections of the mediodorsal thalamic nucleus in the rat, related to the mediodorsal-prefrontal topography. *Neuroscience* **24**, 379–431.

Groenewegen HJ & Berendse HW (1994). The specificity of the 'nonspecific' midline and intralaminar thalamic nuclei. *Trends Neurosci* **17**, 52–57.

Gunaydin LA, Yizhar O, Berndt A, Sohal VS, Deisseroth K & Hegemann P (2010). Ultrafast optogenetic control. *Nat Neurosci* **13**, 387–392.

Herkenham M (1979). The afferent and efferent connections of the ventromedial thalamic nucleus in the rat. *J Comp Neurol* **183**, 487–517.

Kemp JM & Powell TP (1971). The termination of fibres from the cerebral cortex and thalamus upon dendritic spines in the caudate nucleus: a study with the Golgi method. *Philos Trans R Soc Lond B Biol Sci* **262**, 429–439.

Kinomura S, Larsson J, Gulyas B & Roland PE (1996). Activation by attention of the human reticular formation and thalamic intralaminar nuclei. *Science* **271**, 512–515.

Kitai ST, Kocsis JD, Preston RJ & Sugimori M (1976). Monosynaptic inputs to caudate neurons identified by intracellular injection of horseradish peroxidase. *Brain Res* **109**, 601–606.

Kramer PF, Christensen CH, Hazelwood LA, Dobi A, Bock R, Sibley DR, Mateo Y & Alvarez VA (2011). Dopamine D2 receptor overexpression alters behavior and physiology in Drd2-EGFP mice. *J Neurosci* **31**, 126–132.

Kreitzer AC & Malenka RC (2005). Dopamine modulation of state-dependent endocannabinoid release and long-term depression in the striatum. *J Neurosci* **25**, 10537–10545.

Kreitzer AC & Malenka RC (2007). Endocannabinoid-mediated rescue of striatal LTD and motor deficits in Parkinson's disease models. *Nature* **445**, 643–647.

Kreitzer AC & Malenka RC (2008). Striatal plasticity and basal ganglia circuit function. *Neuron* **60**, 543–554.

Krettek JE & Price JL (1977). The cortical projections of the mediodorsal nucleus and adjacent thalamic nuclei in the rat. *J Comp Neurol* **171**, 157–191.

Lacey CJ, Bolam JP & Magill PJ (2007). Novel and distinct operational principles of intralaminar thalamic neurons and their striatal projections. *J Neurosci* **27**, 4374–4384.

Lacey CJ, Boyes J, Gerlach O, Chen L, Magill PJ & Bolam JP (2005). GABA(B) receptors at glutamatergic synapses in the rat striatum. *Neuroscience* **136**, 1083–1095.

Lapper SR & Bolam JP (1992). Input from the frontal cortex and the parafascicular nucleus to cholinergic interneurons in the dorsal striatum of the rat. *Neuroscience* **51**, 533–545.

Lee CC & Sherman SM (2011). Drivers and modulators in the central auditory pathways. *Front Neurosci* **4**, 79–86.

Losonczy A, Makara JK & Magee JC (2008). Compartmentalized dendritic plasticity and input feature storage in neurons. *Nature* **452**, 436–441.

Macchi G, Bentivoglio M, Molinari M & Minciacchi D (1984). The thalamo-caudate versus thalamo-cortical projections as studied in the cat with fluorescent retrograde double labeling. *Exp Brain Res* **54**, 225–239.

Mahon S, Deniau JM & Charpier S (2004). Corticostriatal plasticity: life after the depression. *Trends Neurosci* **27**, 460–467.

Mathur BN, Capik NA, Alvarez VA & Lovinger DM (2011). Serotonin induces long-term depression at corticostriatal synapses. *J Neurosci* **31**, 7402–7411.

Matsumoto N, Minamimoto T, Graybiel AM & Kimura M (2001). Neurons in the thalamic CM-Pf complex supply striatal neurons with information about behaviorally significant sensory events. *J Neurophysiol* **85**, 960–976.

Minamimoto T, Hori Y & Kimura M (2005). Complementary process to response bias in the centromedian nucleus of the thalamus. *Science* **308**, 1798–1801.

Moss J & Bolam JP (2008). A dopaminergic axon lattice in the striatum and its relationship with cortical and thalamic terminals. *J Neurosci* **28**, 11221–11230.

Nelson AB, Hang GB, Grueter BA, Pascoli V, Luscher C, Malenka RC & Kreitzer AC (2012). A comparison of striatal-dependent behaviors in wild-type and hemizygous Drd1a and Drd2 BAC transgenic mice. *J Neurosci* **32**, 9119–9123.

Pawlak V & Kerr JN (2008). Dopamine receptor activation is required for corticostriatal spike-timing-dependent plasticity. *J Neurosci* **28**, 2435–2446.

Petreanu L, Huber D, Sobczyk A & Svoboda K (2007). Channelrhodopsin-2-assisted circuit mapping of long-range callosal projections. *Nat Neurosci* **10**, 663–668.

Plotkin JL, Day M & Surmeier DJ (2011). Synaptically driven state transitions in distal dendrites of striatal spiny neurons. *Nat Neurosci* **14**, 881–888.

Popescu AT, Saghyan AA & Pare D (2007). NMDA-dependent facilitation of corticostriatal plasticity by the amygdala. *Proc Natl Acad Sci U S A* **104**, 341–346.

Raju DV, Shah DJ, Wright TM, Hall RA & Smith Y (2006). Differential synaptology of vGluT2-containing thalamostriatal afferents between the patch and matrix compartments in rats. *J Comp Neurol* **499**, 231–243.

Rudkin TM & Sadikot AF (1999). Thalamic input to parvalbumin-immunoreactive GABAergic interneurons: organization in normal striatum and effect of neonatal decortication. *Neuroscience* **88**, 1165–1175.

Sadikot AF, Parent A, Smith Y & Bolam JP (1992). Efferent connections of the centromedian and parafascicular thalamic nuclei in the squirrel monkey: a light and electron microscopic study of the thalamostriatal projection in relation to striatal heterogeneity. *J Comp Neurol* **320**, 228–242.

Shen W, Flajolet M, Greengard P & Surmeier DJ (2008). Dichotomous dopaminergic control of striatal synaptic plasticity. *Science* **321**, 848–851.

Sherman SM & Guillery RW (1998). On the actions that one nerve cell can have on another: distinguishing "drivers" from "modulators". *Proc Natl Acad Sci U S A* **95**, 7121–7126.

Shindou T, Ochi-Shindou M & Wickens JR (2011). A Ca(2+) threshold for induction of spike-timing-dependent depression in the mouse striatum. *J Neurosci* **31**, 13015–13022.

Sidibé M & Smith Y (1999). Thalamic inputs to striatal interneurons in monkeys: synaptic organization and co-localization of calcium binding proteins. *Neuroscience* **89**, 1189–1208.

Smeal RM, Gaspar RC, Keefe KA & Wilcox KS (2007). A rat brain slice preparation for characterizing both thalamostriatal and corticostriatal afferents. *J Neurosci Methods* **159**, 224–235.

Smeal RM, Keefe KA & Wilcox KS (2008). Differences in excitatory transmission between thalamic and cortical afferents to single spiny efferent neurons of rat dorsal striatum. *Eur J Neurosci* **28**, 2041–2052.

Smith Y, Raju D, Nanda B, Pare JF, Galvan A & Wichmann T (2009). The thalamostriatal systems: anatomical and functional organization in normal and parkinsonian states. *Brain Res Bull* **78**, 60–68.

Smith Y, Raju DV, Pare JF & Sidibe M (2004). The thalamostriatal system: a highly specific network of the basal ganglia circuitry. *Trends Neurosci* **27**, 520–527.

Surmeier DJ, Ding J, Day M, Wang Z & Shen W (2007). D1 and D2 dopamine-receptor modulation of striatal glutamatergic signaling in striatal medium spiny neurons. *Trends Neurosci* **30**, 228–235.

Threlfell S, Lalic T, Platt NJ, Jennings KA, Deisseroth K & Cragg SJ (2012). Striatal dopamine release is triggered by synchronized activity in cholinergic interneurons. *Neuron* **75**, 58–64.

Van der Werf YD, Witter MP & Groenewegen HJ (2002). The intralaminar and midline nuclei of the thalamus. Anatomical and functional evidence for participation in processes of arousal and awareness. *Brain Res Brain Res Rev* **39**, 107–140.

Wang Z, Kai L, Day M, Ronesi J, Yin HH, Ding J, Tkatch T, Lovinger DM & Surmeier DJ (2006). Dopaminergic control of corticostriatal long-term synaptic depression in medium spiny neurons is mediated by cholinergic interneurons. *Neuron* **50**, 443–452.

Wei P, Smeyne RJ, Bao D, Parris J & Morgan JI (2007). Mapping of Cbln1-like immunoreactivity in adult and developing mouse brain and its localization to the endolysosomal compartment of neurons. *Eur J Neurosci* **26**, 2962–2978.

Xu ZC, Wilson CJ & Emson PC (1991). Restoration of thalamostriatal projections in rat neostriatal grafts: an electron microscopic analysis. *J Comp Neurol* **303**, 22–34.

Yin HH & Knowlton BJ (2006). The role of the basal ganglia in habit formation. *Nat Rev Neurosci* **7**, 464–476.

Zhang YP & Oertner TG (2007). Optical induction of synaptic plasticity using a light-sensitive channel. *Nat Methods* **4**, 139–141.

Author contributions

T.J.E., M.C. and J.P.B. designed and supervised the project; T.J.E., J.H. and P.K. performed the experiments, analysed and interpreted the data; T.J.E., M.C. and J.P.B. drafted the article and revised it critically. All authors approved the final version.

Acknowledgements

This research was supported by the European Community (FP7: HEALTH-F2-2008-201716) and the Medical Research Council, UK (grant U138164490). We thank K. Newton, L. Norman, G. Hazel, B. Micklem, C. Johnson and K. Whitworth for technical assistance. We are grateful to K. C. Nakamura and P. J. Magill for advice on immunolabelling for cerebellin-1 and preproenkephalin. We thank K. Deisseroth for the gift of the ChR2 and ChETA constructs and J. Morgan for the gift of the cerebellin-1 antibody.